ResearchGate

See discussions, stats, and author profiles for this publication at: https://www.researchgate.net/publication/259969376

Insights into Li + Migration Pathways in α-Li 3 VF 6 : A First-Principles Investigation

ARTICLE *in* JOURNAL OF PHYSICAL CHEMISTRY LETTERS · NOVEMBER 2012

Impact Factor: 7.46 · DOI: 10.1021/jz3014198

CITATIONS
3

READS
12

4 AUTHORS, INCLUDING:

Mazharul Mohammad Islam
University of Bonn
46 PUBLICATIONS **516** CITATIONS
SEE PROFILE

Martin Wilkening
Graz University of Technology
119 PUBLICATIONS **1,564** CITATIONS
SEE PROFILE

Paul Heitjans
Leibniz Universität Hannover
265 PUBLICATIONS **3,624** CITATIONS
SEE PROFILE

Available from: Mazharul Mohammad Islam
Retrieved on: 30 January 2016

THE JOURNAL OF PHYSICAL CHEMISTRY Letters

Letter

pubs.acs.org/JPCL

Insights into Li^+ Migration Pathways in α-Li_3VF_6: A First-Principles Investigation

Mazharul M. Islam,*[,†,⊥] Martin Wilkening,[‡,⊥] Paul Heitjans,[§,⊥] and Thomas Bredow*[,†,⊥]

[†]Mulliken Center for Theoretical Chemistry, Institut für Physikalische und Theoretische Chemie, Universität Bonn, Beringstraße 4, D-53115 Bonn, Germany

[‡]Institute for Chemistry and Technology of Materials, Graz University of Technology, Stremayrgasse 9, A-8010 Graz

[§]Institute of Physical Chemistry and Electrochemistry and [⊥]ZFM – Center for Solid State Chemistry and New Materials, Leibniz University Hannover, Callinstraße 3-3a, D-30167 Hannover, Germany

ABSTRACT: Magnetic, structural, and defect properties of lithium vanadium hexafluoride (α-Li_3VF_6) are investigated theoretically with periodic quantum chemical methods. It is found that the ferromagnetic phase is more stable than the antiferromagnetic phase. The crystal structure contains three inequivalent Li sites (Li(1), Li(2), and Li(3)), where Li(1) occupies the middle position of the triplet Li(2)–Li(1)–Li(3). The calculated Li vacancy formation energies show that vacancy formation is preferred for the Li(1) and Li(3) sites compared to the Li(2) position. The Li exchange processes between Li(1) ↔ Li(3), Li(1) ↔ Li(2), and Li(2) ↔ Li(3) are studied by calculating the Li^+ migration between these sites using the climbing-image nudged elastic band approach. It is observed that Li exchange in α-Li_3VF_6 may take place in the following order: Li(1) ↔ Li(3) > (Li(1) ↔ Li(2) > Li(2) ↔ Li(3). This is in agreement with recently published results obtained from 1D and 2D ^{6}Li exchange nuclear magnetic resonance spectroscopy.

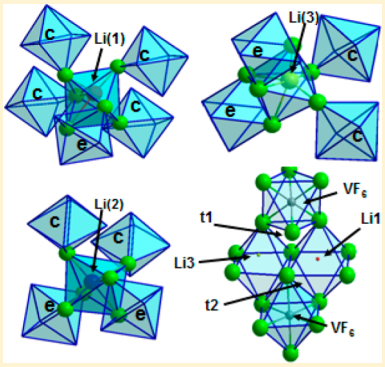

SECTION: Molecular Structure, Quantum Chemistry, and General Theory

Li-containing transition-metal fluorides have attracted considerable attention because of their practical applications in energy storage and energy conversion.[1] The metal–fluorine bond stabilizes the energy of antibonding d orbitals of the transition-metal ions more than the metal–oxygen bond. Consequently, this increases the voltage of lithium insertion.[2] Therefore, besides the Li-containing transition-metal oxides, the corresponding fluorides are regarded as promising candidates to be used as cathode materials in high-energy-density rechargeable batteries.[2−7] Regarding possible applications in the field of energy conversion, transition-metal fluorides are considered to act as, for example, electrolytes in fuel cells or transparent electrodes in solar cells.[1]

Besides electrochemical properties and chemical stability, Li^+ migration in the electrode materials plays a crucial role in determining the performance of a lithium ion battery. Recently, Li jump rates and Li migration pathways in polycrystalline α-Li_3VF_6 have been probed by variable-temperature 1D and 2D exchange magic angle spinning (MAS) nuclear magnetic resonance (NMR) spectroscopy by Wilkening et al.[8] The α-modification of Li_3VF_6 crystallizes with orthorhombic symmetry (space group *Pna*21) and has 40 atoms in the unit cell (Z = 4). The measured lattice parameters are a = 9.59 Å, b = 8.48 Å, and c = 5.03 Å. In α-Li_3VF_6, there are three crystallographically different and magnetically inequivalent Li sites[9] fully occupied by Li cations (labeled as Li(1), Li(2), and Li(3) in Figure 1a). Li(1) occupies the central position of the triplet Li(2)–Li(1)–Li(3), as shown in Figure 1b. Results from NMR spectroscopy[8] suggest that the most probable exchange processes involve the face-shared LiF_6 octahedra with exchange between either Li(1) ↔ Li(3) or Li(1) ↔ Li(2). The contour plots of mixing-time-dependent 2D exchange MAS NMR spectra reveal that the Li(1) ↔ Li(3) exchange process in α-Li_3VF_6 is found to be somewhat faster than Li exchange between the sites Li(1) and Li(2).

To our knowledge, there are no previous theoretical investigations on the defect and transport properties of α-Li_3VF_6. In the present study, a theoretical investigation of the structural and defect properties of the ternary fluoride is presented. Both Li vacancy defects and Li migration in α-Li_3VF_6 were studied by using first-principles methods and periodic supercell models. The activation energies of Li^+ ion migration are calculated for different diffusion pathways.

Bulk and defect properties of α-Li_3VF_6 were calculated using the Perdew–Burke–Ernzerhof (PBE) functional[10,11] based on the generalized gradient approximation (GGA) as implemented in the plane wave program VASP.[12−14] The projector-augmented wave (PAW) method[15,16] was used for the core–electron representation. According to preliminary test calculations, in this study, we used a converged value of the cutoff energy E_{cut} = 520 eV. The integration in reciprocal space was performed with a 2 × 2 × 4 Monkhorst–Pack grid.[17] The

Received: September 14, 2012
Accepted: October 9, 2012

 © XXXX American Chemical Society dx.doi.org/10.1021/jz3014198 | *J. Phys. Chem. Lett.* 2012, 3, 3120–3124

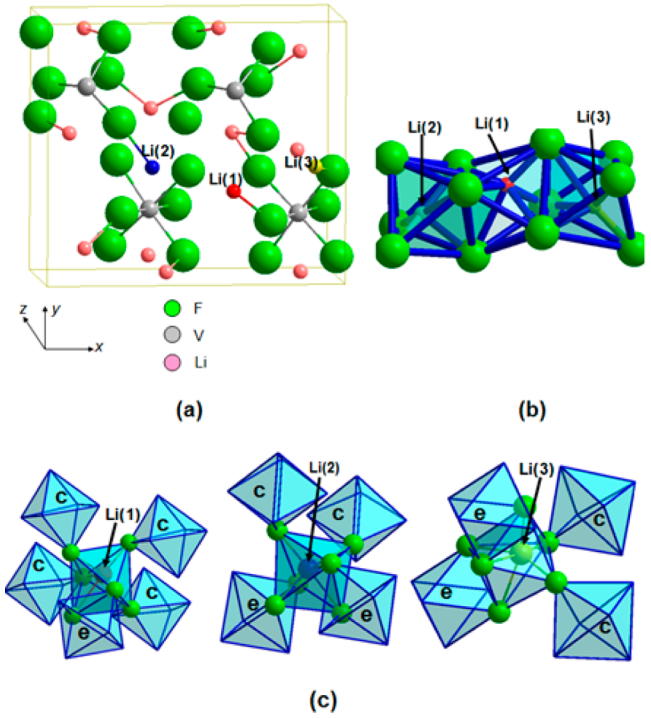

Figure 1. (a) The unit cell of α-Li_3VF_6 showing the Li(2)−Li(1)−Li(3) triplet. (b) Local structure of the Li(2)−Li(1)−Li(3) triplet. (c) Number of VF_6 octahedra surrounding the LiF_6 octahedra for Li(1), Li(2), and Li(3); e and c denote edge and corner sharing, respectively. The green spheres represent fluorine atoms.

defective structures were simulated by a $Li_{12}V_4F_{24}$ supercell. The transition-state search for the migration processes was conducted with the climbing-image nudged elastic band (cNEB)[18] method as implemented in VASP. Vibrational analysis calculations were performed to verify the true local minima and saddle point character of the optimized geometries. No imaginary frequencies were obtained for the local minimum structures, whereas one imaginary frequency was observed for the transition-state structures. In order to study the effect of local electron exchange on the electronic structure and defect energetics, additional investigations were performed using the DFT+U approach, where the value of U was chosen as 5 eV.[19]

In all cases, full optimization of the fractional coordinates and the lattice parameters was performed. The nature of the magnetic ground state was investigated by considering ferromagnetic and antiferromagnetic structures. For the antiferromagnetic structure, different stacking sequences of spin-up and spin-down moments are possible. Our investigation shows that the ferromagnetic structure represents the magnetic ground state, which is lower in energy by 16 (DFT) and 27 meV (DFT+U) compared to the antiferromagnetic phase. Therefore, for all following steps of our study, we have considered the ferromagnetic phase of α-Li_3VF_6.

As shown in Table 1, the optimized fractional coordinates are in good agreement with the experimental data obtained from Rietveld refinement.[8] The calculated lattice parameters (a = 9.51, b = 8.43, and c = 4.95 Å by the DFT approach and a = 9.64, b = 8.53, and c = 5.10 Å by the DFT+U approach) are in good agreement with experimental values;[8] the deviation is less than 0.08 Å.

The structural analysis[8] shows that the Li(1)F_6 octahedron is surrounded by five VF_6 octahedra. Four of them are corner-

Table 1. Comparison of Calculated Atomic Fractional Coordinates with Experimental Data from Rietveld Refinement (R.R.)[8]

	x		y		z	
atom	R.R.	calc.	R.R.	calc.	R.R.	calc.
V(1)	0.126	0.129	0.247	0.240	0.000	0.000
F(1)	0.234	0.229	0.060	0.061	0.143	0.148
F(2)	0.027	0.023	0.230	0.246	0.355	0.331
F(3)	0.246	0.239	0.238	0.233	0.677	0.683
F(4)	0.015	0.023	0.409	0.407	0.852	0.850
F(5)	0.245	0.249	0.371	0.389	0.172	0.185
F(6)	0.020	0.010	0.089	0.084	0.830	0.823
Li(1)	0.375	0.375	0.349	0.356	0.507	0.509
Li(2)	0.105	0.102	0.457	0.449	0.497	0.501
Li(3)	0.354	0.351	0.546	0.549	0.002	0.004

shared (labeled as c), and one is edge-shared (labeled as e), as shown in Figure 1c. Li(2)F_6 and Li(3)F_6 are surrounded by four VF_6 octahedra (two corner-shared and two edge-shared). The Li−F−V angles substantially deviate from 180°.[8] Compared to the experimental values, the highest deviations of the calculated Li−F, V−F, and Li−V bond distances and Li−F−V bond angles are ±0.05 Å and ±2°, respectively.

A systematic investigation was performed for the cation vacancy formation energy E_{de}(V) and the effect of relaxation of defective α-Li_3VF_6. One neutral Li atom was removed from the cell to create the defective system. This led to an open-shell electronic structure with one unpaired electron per cell. Therefore, the calculations were performed using the spin-polarized Kohn−Sham method. A full optimization of atomic fractional coordinates was performed by fixing the optimized lattice parameters from the stoichiometric bulk optimization. The formation energy of a Li vacancy E_{de}(V) was calculated according to the following equation

$$E_{de}(V) = E^{SCM}(V) + E(Li) - E^{SCM}$$

Here, E^{SCM}(V) and E^{SCM} denote the total energy of the supercell model with and without vacancy, respectively, while E(Li) represents the energy of the free Li atom.

The calculated point defect formation energies for Li(1), Li(2), and Li(3) are 4.49, 4.60, and 4.51 eV, respectively, by the DFT method and 5.11, 5.24, and 5.14 eV, respectively, by the DFT+U method. Although the DFT+U approach gives slightly larger values compared to the DFT approach, both methods give the same trend for the defect formation energy.

The electronic properties for the nondefective and defective systems were calculated by means of density of states (DOS) and spin density distribution calculations. There is no experimental value of the band gap (E_g) for α-Li_3VF_6; therefore, we compare the calculated values with the PW1PW hybrid[20] value in this study. The calculated PW1PW E_g is 3.54 eV. As expected, the DFT method underestimates E_g (1.80 eV, Figure 2a), whereas the DFT+U approach gives good agreement (E_g = 3.40 eV, Figure 2b) with the PW1PW method. The PBE DOS calculations of the Li defective supercell show that the electronic levels (occupied d states of vanadium) that arise from Li vacancy formation lie very close to the bottom of the conduction band (as marked by arrow in Figure 2c), resulting in further narrowing the band gap. However, standard DFT functionals are unable to properly describe the localization of unpaired electrons in transition-metal systems. The self-interaction error causes an artificially high repulsion between

dx.doi.org/10.1021/jz3014198 | J. Phys. Chem. Lett. 2012, 3, 3120−3124

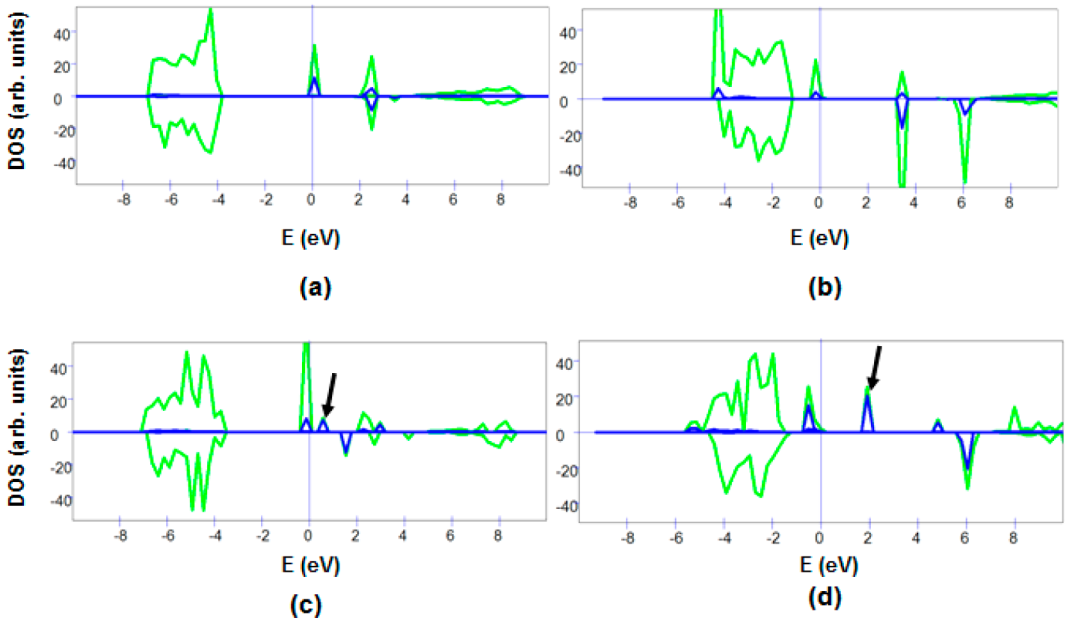

Figure 2. Electronic properties of α-Li_3VF_6. Total DOS (green curves) and projected DOS of V 3d states (blue curves) for the nondefective system by DFT (a) and DFT+U (b) approaches and for the Li defective system by DFT (c) and DFT+U (d) approaches. The occupied defect states are marked by arrows.

electrons in localized states, often resulting in an excessive delocalization.[21,22] At the GGA+U level, the picture is different because the occupied defect states are now below the bottom of the conduction band (see Figure 2d), indicating a more pronounced localization. The spin density calculated with DFT +U is localized on one vanadium atom, which is the nearest to the Li defect, whereas it is distributed on the neighboring four vanadium atoms with the DFT approach. It should be noted that although the electron localization affects the size of the band gap, it does not affect the energetics of the defective systems. Also, the trend in stability of Li defect formation in different Li sites obtained with the DFT and the DFT+U methods is the same. Therefore, the transition-state search calculations for the Li^+ migration using the cNEB approach are performed only at the GGA level.

As mentioned above, 2D exchange ^{6}Li MAS NMR spectroscopy[8] suggests that the most probable exchange processes involve the face-shared LiF_6 octahedra, leading to a one-step, direct hopping process. It turned out that the Li exchange rate ascribed to the Li(1) ↔ Li(3) process was found to be slightly larger than that of the corresponding Li(1) ↔ Li(2) process. The NMR results show that Li exchange between Li(2) and Li(3), even when two-step migration pathways are regarded, turned out to be less favorable.

There are several types of migration pathways such as (a) Li^+ migration through the triangular F−F−F face of two shared LiF_6 octahedra (Li(1) ↔ Li(2), Li(1) ↔ Li(3), Li(3)′ ↔ Li(1)′, or Li(1)′ ↔ Li(2)′, as shown in Figure 3); (b) Li^+ migration involving the tetrahedral void connecting two LiF_6 octahedra according to a two-step process (Li(1) ↔ Li(3)″ or Li(3) ↔ Li(1)″, as shown in Figure 3); and (c) direct Li migration via an empty site (Li(2) ↔ Li(3)).

The calculated activation energies (E_A) for all of these migration pathways are listed in Table 2. Our calculated E_A for the direct Li exchange between Li(1) ↔ Li(2) ranges from 0.28 to 0.35 eV, and that for the Li exchange between Li(1) ↔ Li(3) is 0.20 eV. Therefore, Li exchange between Li(1) ↔ Li(3) is

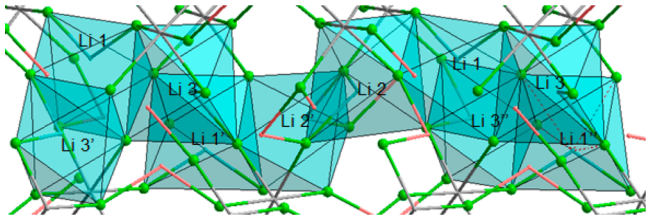

Figure 3. Local structure showing the various possible migration pathways considered.

Table 2. Calculated Activation Energies E_A (eV) for the Different Li^+ Migration Pathways Considered

	type	E_A
one-step process via face	Li(1)−Li(2)	0.35
	Li(1) −Li(3)	0.20
	Li(1)′−Li(2)′	0.28
	Li(3)′−Li(1)′	0.20
via tetrahedral space	Li(1)−Li(3)″	0.16
	Li(3)−Li(1)″	0.17
via empty site	Li(2)−Li(3)	0.71
	Li(3)−Li(2)′	0.75

energetically more favorable than that between Li(1) ↔ Li(2). This is in agreement with the observations by NMR spectroscopy.[8]

Apart from these one-step, direct diffusion pathways through the F−F−F triangular face, the Li(1) ↔ Li(3) exchange can also occur via a two-step migration pathway. In this case, Li(1) migrates to Li(3) and vice versa through an intermediate, as shown in Figure 4a. The structural analysis shows that Li(1) can reach the empty Li(3)″ site via the vacant tetrahedral void 1 (t1) or via the tetrahedral void 2 (t2), as shown in Figure 4b. t1 is connected by edge sharing of two F atoms of a neighboring VF_6 octahedron, whereas t2 is connected via face sharing of three F atoms of the VF_6 octahedron. The analysis of the intermediate structure for the exchange between Li(1) and

dx.doi.org/10.1021/jz3014198 | J. Phys. Chem. Lett. 2012, 3, 3120−3124

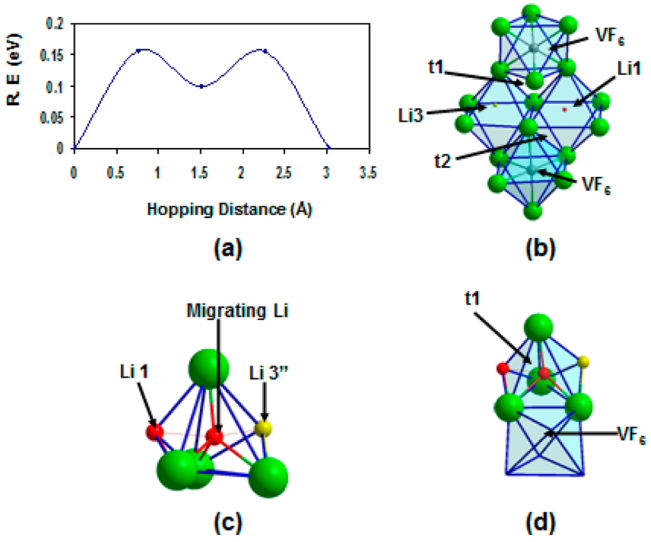

Figure 4. (a) Potential energy curve for a Li ion migration pathway using the tetrahedral void connecting the Li(1) and Li(3)″ sites, (b) local structure showing the location of the t1 and t2 tetrahedra, (c) intermediate structure showing the migrating Li and the arbitrary location of Li(1) and Li(3)″, and (d) the intermediate structure illustrating the Li migration through the t1 intermediate.

Li(3)″ shows that Li^+ migrates via t1 rather than t2 (Figure 4c and d). This can be attributed to the smaller repulsive Li^+–V^{3+} interaction for the former case, as also proposed in the NMR study of ref 8. The activation energy for this two-step migration process is very small, 0.16–0.17 eV. The exchange between Li(2) and Li(3) can occur via an empty site with a one-step, direct migration pathway. The activation energy for this migration pathway is relatively high (0.71–0.75 eV). Here, it should be noted that there is a systematic effect of electron localization on all of the migration pathways; thereby, the activation barriers for all pathways with DFT+U may be slightly larger compared to those with the DFT approach.

Comparing the migration processes considered here, we obtained the following ordering of activation barriers, E_A(Li(1) ↔ Li(3)″) < E_A(Li(1) ↔ Li(2)) < E_A(Li(2) ↔ Li(3)). Therefore, Li(1) and Li(3) ions are involved in the most favorable diffusion pathway, which is in accordance with results from 2D MAS NMR spectroscopy.[8] The calculations also confirm the assignment of the three distinct ^{6}Li NMR lines presented in ref 8. This assignment is based on the combination of (i) geometric considerations, (ii) results from mixing-time-dependent 2D MAS NMR experiments, as well as (iii) the relevant spin density transfer mechanisms, which interrelate the experimentally probed NMR shift with the extent of spin density transferred from the vanadium centers to the Li sites.

In summary, we have studied the structural and energetic properties of stoichiometric and defective α-Li_3VF_6 with the density functional method PBE-GGA. The optimized fractional coordinates are in good agreement with the experimental Rietveld refinement data. The calculated lattice parameters, bond distances, and bond angles are in well accord with experimental data. The calculated defect formation energies for Li(1), Li(2), and Li(3) (4.49, 4.60, and 4.51 eV at the PBE level and 5.11, 5.24, and 5.14 eV at the PBE+U level) indicate that the delithiation of Li(1) and Li(3) is slightly less energetically costly than that of Li(2). In any case, α-Li_3VF_6 can be considered as a high-voltage cathode material for lithium ion batteries. Several possibilities of Li^+ ion migration pathways have been investigated by Li exchange between Li(1) ↔ Li(2), Li(1) ↔ Li(3), and Li(2) ↔ Li(3). The calculated activation energies indicate that the most likely Li^+ migration pathway involves one-step direct Li exchange between Li(1) and Li(3) as well as two-step exchange via the tetrahedral intermediate t1. t1 is connected to a neighboring VF_6 octahedron by edge sharing. The present investigation confirms both the assignment of the NMR lines to the Li sites in α-Li_3VF_6, see ref 8, and the site-specific dynamic properties derived from temperature-variable 1D and 2D exchange NMR spectroscopy.[8] The rather small activation barriers calculated for the direct Li(1) ↔ Li(3) hopping process (0.16–0.17 eV) are in agreement with the rapid Li diffusion process probed by NMR. In general, facile Li^+ hopping is beneficial when fluorides are intended to be used as electrode materials in lithium ion batteries.

AUTHOR INFORMATION

Corresponding Author

*E-mail: rana-islam@thch.uni-bonn.de (M.M.I.); bredow@thch.uni-bonn.de (T.B.).

Notes

The authors declare no competing financial interest.

ACKNOWLEDGMENTS

M.M.I. is grateful to the Deutsche Forschungsgemeinschaft (DFG) for the postdoctorate funding within the Research Unit 1277 molife "Mobilität von Li-Ionen in Festkörpern".

REFERENCES

(1) Amatucci, G. G.; Pereira, N. Fluoride Based Electrode Materials for Advanced Energy Storage Devices. *J. Fluorine Chem.* **2007**, *128*, 243–262.

(2) Dompablo, M. E. A-de; Amador, U; Tarascon, J.-M. A Computational Investigation on Fluorinated-Polyanionic Compounds As Positive Electrode for Lithium Batteries. *J. Power Sources* **2007**, *174*, 1251–1257.

(3) Barker, J.; Saidi, M. Y.; Swoyer, J. L. Electrochemical Insertion Properties of the Novel Lithium Vanadium Fluorophosphate, $LiVPO_4F$. *J. Electrochem. Soc.* **2003**, *150*, A1394–A1398.

(4) Yin, S.-C.; Herle, P. S.; Higgins, A; Taylor, N. J.; Makimura, Y.; Nazar, L. F. Dimensional Reduction: Synthesis and Structure of Layered $Li_5M(PO_4)_2F_2$ (M = V, Cr). *Chem. Mater.* **2006**, *18*, 1745–1752.

(5) Sorensen, E. M.; Izumi, H. K.; Vaughey, J. T.; Stern, C. L.; Poeppelmeir, K. R. $Ag_4V_2O_6F_2$: An Electrochemically Active and High Silver Density Phase. *J. Am. Chem. Soc.* **2005**, *127*, 6347–6352.

(6) Makimura, Y.; Cahill, L. S.; Iriyama, Y.; Goward, G. R.; Nazar, L. F. Layered Lithium Vanadium Fluorophosphate, $Li_5V(PO_4)_2F_2$: A 4 V Class Positive Electrode Material for Lithium-Ion Batteries. *Chem. Mater.* **2008**, *20*, 4240–4248.

(7) Cahill, L. S.; Iriyama, Y.; Nazar, L. F.; Goward, G. R. Synthesis of $Li_4V(PO_4)_2F_2$ and ^{6,7}Li NMR Studies of Its Lithium Ion Dynamics. *J. Mater. Chem.* **2010**, *20*, 4340–4346.

(8) Wilkening, M.; Romanova, E. E.; Nakhal, S.; Weber, D.; Lerch, M.; Heitjans, P. Time-Resolved and Site-Specific Insights into Migration Pathways of Li^+ in α-Li_3VF_6 by ^{6}Li 2D Exchange MAS NMR. *J. Chem. Phys. C* **2010**, *114*, 19083–19088.

(9) Kohl, J.; Wiedemann, D.; Nakhal, S.; Bottke, P.; Ferro, N.; Bredow, T.; Kemnitz, E.; Wilkening, M.; Heitjans, P.; Lerch, M. Synthesis of Ternary Transition Metal Fluorides Li_3MF_6 via a Sol–Gel Route As Candidates for Cathode Materials in Lithium-Ion Batteries. *J. Mater. Chem.* **2012**, *22*, 15819–15827.

(10) Perdew, J. P.; Burke, K.; Ernzerhof, M. Generalized Gradient Approximation Made Simple. *Phys. Rev. Lett.* **1996**, *77*, 3865–3868.

(11) Perdew, J. P.; Burke, K.; Ernzerhof, M. Generalized Gradient Approximation Made Simple. *Phys. Rev. Lett.* **1997**, *78*, 1396−1396.
(12) Kresse, G.; Hafner, J. Ab Initio Molecular Dynamics for Liquid Metals. *Phys. Rev. B* **1993**, *47*, 558−561.
(13) Kresse, G.; Hafner, J. Ab Initio Molecular Dynamics for Open-Shell Transition Metals. *Phys. Rev. B* **1993**, *48*, 13115−13118.
(14) Kresse, G.; Hafner, J. Ab Initio Molecular-Dynamics Simulation of the Liquid-Metal−Amorphous-Semiconductor Transition in Germanium. *Phys. Rev. B* **1994**, *49*, 14251−14269.
(15) Kresse, G.; Joubert, J. From Ultrasoft Pseudopotentials to the Projector Augmented-Wave Method. *Phys. Rev. B* **1999**, *59*, 1758−1775.
(16) Blöchl, P. E. Projector Augmented-Wave Method. *Phys. Rev. B* **1994**, *50*, 17953−17979.
(17) Monkhorst, H. J.; Pack, J. D. Special Points for Brillouin-Zone Integrations. *Phys. Rev.* **1976**, *13*, 5188−5192.
(18) Jónsson, H.; Mills, G.; Jacobsen, K. W. In *Classical and Quantum Dynamics in Condensed Phase Simulations*; Berne, B. J., Ciccotti, G., Coker, D. F.; Eds.; World Scientific: Singapore, 1998; p 385.
(19) We have determined a value of U = 5 eV as leading to the optimal agreement between theory and experiment for a wide range of physical properties such as equilibrium volume, magnetic moment, and band gap. The ground-state properties have been determined for Coulomb parameters ranging from $U - J$ = 0 eV (GGA limit) up to $U - J$ = 8 eV, together with a constant exchange parameter J = 1 eV. We have used the PW1PW hybrid method[20] for the band gap calculation as reference. The magnetic moment and the band gap remain below the reference values, whereas the equilibrium atomic volume is overestimated slightly compared to experiment. A value of U = 5 eV leads to an acceptable compromise between the structural and the electronic properties.
(20) Bredow, T.; Gerson, A. R. Effect of Exchange and Correlation on Bulk Properties of MgO, NiO, and CoO. *Phys. Rev. B* **2000**, *61*, 5194−5201.
(21) Islam., M. M.; Calatayud, M.; Pacchioni, G. Hydrogen Adsorption and Diffusion on the Anatase TiO_2(101) Surface: A First-Principles Investigation. *J. Phys. Chem. C* **2011**, *115*, 6809−6814.
(22) Islam., M. M.; Bredow, T.; Heitjans, P. The Ionic Conductivity in Lithium-Boron Oxide Materials and Its Relation to Structural, Electronic and Defect Properties: Insights from Theory. *J. Phys.: Condens. Matter* **2012**, *24*, 203201−203229.